



Cite this: DOI: 10.1039/d6sd00055j

Development of colorimetric and fluorescent sensor based on a combination of ICT (intramolecular charge transfer) and FRET (Förster resonance energy transfer) for the detection of water

 Kosuke Okutani, Keiichi Imato  and Yousuke Ooyama *

Colorimetric and fluorescent sensors for water are crucial to environmental and quality control monitoring, industrial process, food inspection and so on. Although the optical sensing mechanism of sensors for water has been of considerable concern in analytical chemistry, photochemistry, and photophysics in recent years, a further fundamental study is necessary to provide a direction in molecular design toward creating highly sensitive fluorescent sensors for detecting, quantitating and visualizing a trace amount of water in solids, liquids, or gases. In this work, we have newly designed and synthesized an ICT (intramolecular charge transfer)/FRET (Förster resonance energy transfer)-type colorimetric and fluorescent sensor, pyridine-boron trifluoride complex **KOY-1-BF₃**, where the thienylpyridine-carbazole-based D-(π -A)₂ skeleton and boron-dipyrromethene (BODIPY) skeleton are the ICT-type donor fluorophore and the acceptor fluorophore in the FRET process, respectively. It was found that the addition of water to the **KOY-1-BF₃** solution causes its dissociation into thienylpyridine-carbazole-based D-(π -A)₂ fluorophore **KOY-1** and then the energy transfer from the thienylpyridine-carbazole-based D-(π -A)₂ skeleton to the BODIPY skeleton through the FRET process, and thus resulting in a large pseudo-Stokes shift of 7942 cm⁻¹ (150 nm) and an enhancement of fluorescence emission originating from the BODIPY skeleton as well as the blue-shift of the ICT-based photoabsorption band. Furthermore, in the high water content region, a decrease in the fluorescence intensity was observed due to the formation of hydrogen-bonded proton transfer complex **KOY-1-H₂O** with water molecules, which shows a feeble fluorescence emission property, leading to low FRET efficiency. Consequently, this work is the first report on the development and optical sensing mechanism of an ICT/FRET-type colorimetric and fluorescent sensor for water possessing a large pseudo-Stokes shift.

 Received 16th March 2026,
 Accepted 3rd June 2026

DOI: 10.1039/d6sd00055j

rsc.li/sensors

Introduction

Development of techniques for detecting and quantitating a trace amount of water in solids, liquids, or gases is absolutely essential for not only environmental and quality control monitoring systems and industry, but for establishing new principles in chemistry, chemical engineering, and physics. In fact, various water content measurement techniques based on chromatographic, chemical, electrical, thermogravimetric, or electromagnetic methods have been developed and are widely used in laboratory, industry, and everyday life.^{1,2} On the other hand, if we can create optical methods using colorimetric and fluorescent sensors for water, the technique

allows us not only to perform quick flow analysis with sufficient accuracy and high sensitivity, but also to visually confirm the presence of water in samples and on material surfaces.³⁻¹⁵ For this purpose, various types of colorimetric and fluorescent sensors for water have been designed and developed, based on ICT (intramolecular charge transfer),¹⁶⁻²³ ESIPT (excited state intramolecular proton transfer),²⁴⁻²⁷ PET (photo-induced electron transfer),²⁸⁻⁴⁴ FRET (Förster resonance energy transfer)^{45,46} or solvatofluorochromism (SFC)⁴⁷⁻⁵³ characteristics, which exhibit the photophysical changes in wavelength, intensity, and lifetime of photoabsorption and photoluminescence depending on the water content. Among them, the ICT-type and FRET-type fluorescent sensors make the colorimetric and ratiometric fluorescent measurements possible, which is preferable because the ratio of the photoabsorption and fluorescence intensities at the two wavelengths is independent of the total concentration of the sensor, photobleaching, fluctuations of

Applied Chemistry Program, Graduate School of Advanced Science and Engineering, Hiroshima University, 1-4-1 Kagamiyama, Higashi-Hiroshima 739-8527, Japan. E-mail: yoyama@hiroshima-u.ac.jp



light source intensity, sensitivity of the instrument, and so on.^{54–60} The ICT-type fluorescent sensors generally have a donor- π -acceptor (D- π -A) structure, which is composed of an electron-donating (D) moiety and an electron-accepting (A) moiety linked by a π -conjugated bridge, so that they exhibit an intense photoabsorption band originating from the ICT characteristics from the D to the A moiety. In our previous work, in order to gain insight into a direction in molecular design toward creating an ICT-type colorimetric and fluorescent sensor for the detection of water in solvents, we have designed and developed a D-(π -A)₂-type pyridine-boron trifluoride complex **YNI-2-BF₃** composed of a two thienyl carbazole skeleton as the D- π moiety and two pyridine-boron trifluoride units as the A moiety (Fig. 1).¹⁹ In the low water content region, **YNI-2-BF₃** exhibited a decrease in the ICT-based photoabsorption band with a simultaneous increase in another ICT-based photoabsorption band in shorter-wavelength, and the appearance and enhancement of a fluorescence emission band, which is attributed to the change in the ICT characteristics due to the dissociation of **YNI-2-BF₃** into D-(π -A)₂-type pyridine dye **YNI-2**. Furthermore, in the relatively high water content region, a decrease in the fluorescence intensity was observed due to the formation of the hydrogen-bonded proton transfer complex (PTC) **YNI-2-H₂O** with water molecules, which shows a feeble fluorescence emission property. However, the disadvantage in this ICT-based fluorescence sensing system for water is that the accuracy and sensitivity for the detection and quantification of water is low due to self-quenching and fluorescence detection errors due to a strong spectral overlap between the ICT-based photoabsorption band of **YNI-2-BF₃** and the fluorescence band of **YNI-2**. Meanwhile, in FRET-based fluorescent sensors, the fluorescence emission originates from the acceptor fluorophore *via* an energy transfer process, that is, the FRET process between the photoexcited donor fluorophore and the ground state acceptor fluorophore. Therefore, to achieve effective FRET, a strong overlap between the fluorescence emission spectrum of the donor fluorophore and the photoabsorption spectrum of the acceptor fluorophore is required. The most advantageous features of FRET-type fluorescent sensors is the large pseudo-Stokes shift (SS) between the photoabsorption maximum of donor

fluorophore and the fluorescence maximum of acceptor fluorescence, which leads to an effective avoidance of the self-quenching and fluorescence detection errors due to photoexcitation and scattering lights from the excitation source.

Thus, in this work, in order to provide a direction in molecular design toward creating a ratiometric fluorescent sensor possessing a large SS for the detection of water over a wide range from low water content to high water content in solvents, we have designed and synthesized a new ICT/FRET-type fluorescent sensor, pyridine-boron trifluoride complex **KOY-1-BF₃**, where the thienylpyridine-carbazole-based D-(π -A)₂ skeleton and boron-dipyrromethene (BODIPY) skeleton are the ICT-type donor fluorophore and the acceptor fluorophore in the FRET process, respectively (Fig. 2). It is expected that the addition of water to the **KOY-1-BF₃** solution causes its dissociation into the thienylpyridine-carbazole-based D-(π -A)₂-BODIPY fluorophore **KOY-1** and then the energy transfer from the thienylpyridine-carbazole-based D-(π -A)₂ skeleton to the BODIPY skeleton through the FRET process, and thus resulting in a large pseudo-SS and an enhancement of fluorescence emission originating from the BODIPY skeleton. Moreover, in the relatively high water content region, it may induce the formation of the hydrogen-bonded proton transfer complex (PTC) **KOY-1-H₂O** with water molecules, which shows a feeble fluorescence emission property, leading to a decrease in the fluorescence intensity due to low FRET efficiency. Indeed, this is the first report on the development and optical sensing mechanism of an ICT/FRET-type colorimetric and fluorescent sensor for water,

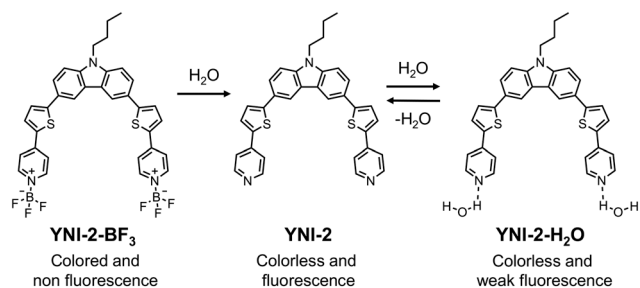


Fig. 1 Proposed mechanisms of ICT-type colorimetric and fluorescent sensor **YNI-2-BF₃** for the detection of water in solvent (our previous work).¹⁹

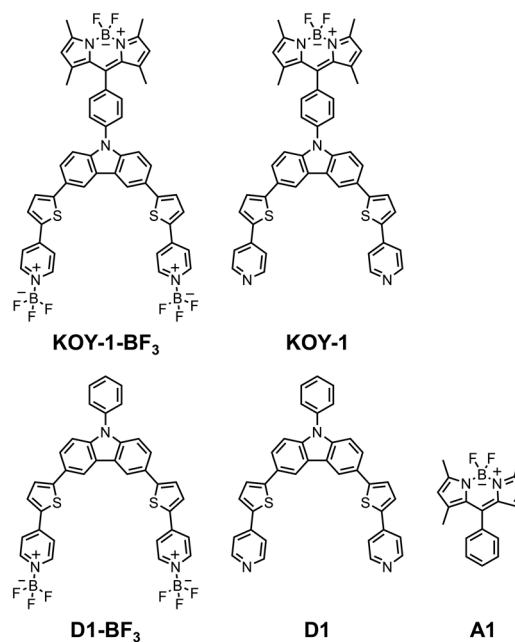


Fig. 2 ICT/FRET-type fluorescent sensor **KOY-1-BF₃**, BODIPY/D-(π -A)₂-type fluorophore **KOY-1**, D-(π -A)₂-type pyridine-boron trifluoride complex **D1-BF₃**, donor fluorophore **D1** and acceptor fluorophore **A1** in the FRET process.



although some ICT/FRET-type fluorescent sensors for H_2O_2 , H_2S and cation species including Cu^{2+} and Zn^{2+} have been developed.^{54–60} Herein, we provide the most promising fluorescence enhancement (turn-on) system for detecting, quantitating and visualizing water.

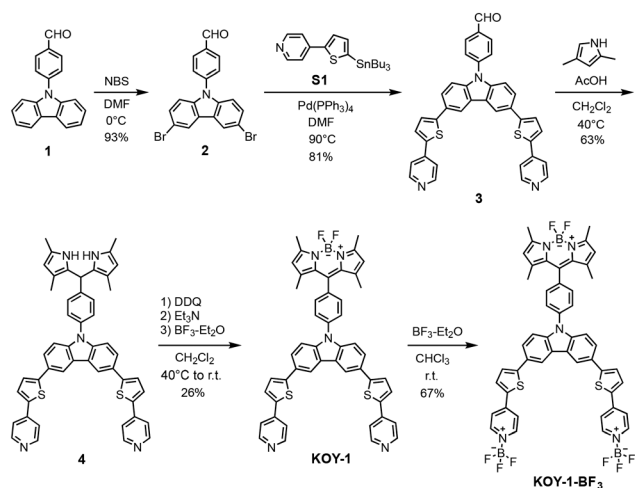
Results and discussion

Synthesis

The ICT/FRET-type fluorescent sensor **KOY-1-BF₃** was synthesized according to a stepwise synthetic protocol (Scheme 1). Compound **1** was prepared according to a reported procedure.⁶¹ Compound **2** was obtained by bromination of compound **1** with *N*-bromosuccinimide (NBS). Compound **3** was obtained by the Stille coupling reaction of compound **2** with (tributylstannyl)thienylpyridine **S1**.⁶² Dipyrromethane derivative **4** was prepared by condensation of compound **3** with 2,4-dimethylpyrrole. BODIPY/D-(π -A)₂-type fluorophore **KOY-1** was prepared by oxidation of compound **4** with 2,3-dichloro-5,6-dicyano-1,4-benzoquinone (DDQ) followed by treatment with $\text{BF}_3\cdot\text{OEt}_2$. Finally, ICT/FRET-type fluorophore **KOY-1-BF₃** was obtained by treating **KOY-1** with $\text{BF}_3\cdot\text{OEt}_2$ and fully characterized by ¹H NMR, ¹¹B NMR, FT-IR, high-resolution mass analysis, and thermogravimetry-differential thermal analysis (TG-DTA), although it was not possible to obtain the ¹³C NMR spectrum to make assignments due to the low solubility of **KOY-1-BF₃** in the solvent. In addition, the D-(π -A)₂-type compound **D1** as a donor fluorophore and its pyridine-boron trifluoride complex **D1-BF₃** were prepared (Fig. 1, see Scheme S1 for the synthesis, SI) and commercially available BODIPY **A1** was used as an acceptor fluorophore, where **D1-BF₃** and **A1** are structural components for **KOY-1-BF₃**.

Photoabsorption and fluorescence properties

The photoabsorption and fluorescence spectra of **D1-BF₃**, **A1**, **KOY-1**, and **KOY-1-BF₃** in acetonitrile and **D1** in THF (because **D1** is poor solubility in acetonitrile) are shown in Fig. 3. **D1**



Scheme 1 Synthesis of **KOY-1-BF₃**.

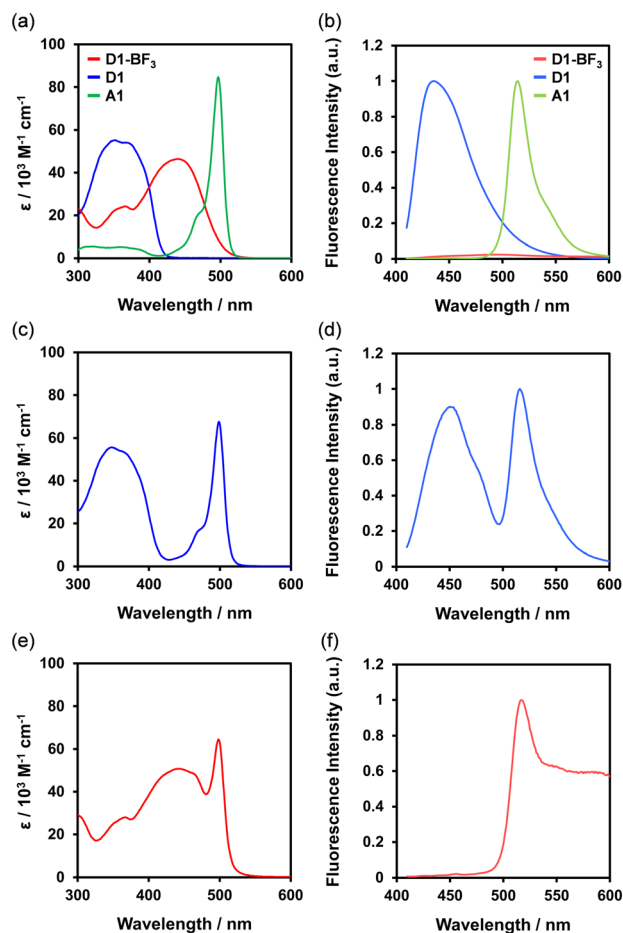


Fig. 3 (a) Photoabsorption and (b) fluorescence ($\lambda^{\text{ex}} = 400$ nm) spectra of **D1** ($c = 2.0 \times 10^{-5}$ M) in THF, and **D1-BF₃** ($c = 2.0 \times 10^{-5}$ M) and **A1** ($c = 2.0 \times 10^{-5}$ M) in acetonitrile. (c) Photoabsorption and (d) fluorescence ($\lambda^{\text{ex}} = 400$ nm) spectra of **KOY-1** ($c = 2.0 \times 10^{-5}$ M) in acetonitrile. (e) Photoabsorption and (f) fluorescence ($\lambda^{\text{ex}} = 400$ nm) spectra of **KOY-1-BF₃** ($c = 2.0 \times 10^{-5}$ M) in acetonitrile.

and **D1-BF₃** show a strong photoabsorption band in the ranges of 300 nm to 420 nm and 400 nm to 500 nm, respectively, which is assigned to the ICT excitation from the electron-donating moiety (carbazole skeleton) to the electron-accepting moiety (pyridyl groups for **D1** and pyridyne-BF₃ units for **D1-BF₃**). The ICT-based photoabsorption maximum ($\lambda_{\text{max}}^{\text{abs}} = 440$ nm) of **D1-BF₃** occurs at a longer wavelength by 68 nm than that ($\lambda_{\text{max}}^{\text{abs}} = 372$ nm) of **D1**, which could be due to the stronger electron-withdrawing ability of pyridyne-BF₃ unit than that of the pyridyl group. The molar extinction coefficient (ϵ_{max}) for the ICT-based $\lambda_{\text{max}}^{\text{abs}}$ (440 nm) of **D1-BF₃** is $46\,400\text{ M}^{-1}\text{ cm}^{-1}$, which is equivalent to that ($52\,800\text{ M}^{-1}\text{ cm}^{-1}$) of **D1**. **A1** shows a strong photoabsorption band ($\lambda_{\text{max}}^{\text{abs}} = 497$ nm, $\epsilon_{\text{max}} = 84\,700\text{ M}^{-1}\text{ cm}^{-1}$) in the range of 420 nm to 520 nm originating from the BODIPY skeleton and a feeble and broad photoabsorption band in the range of 300 nm to 400 nm. On the other hand, **KOY-1** and **KOY-1-BF₃** show two strong photoabsorption bands in the ranges of 300 nm to 420 nm ($\lambda_{\text{max}}^{\text{abs}} = 366$ nm, $\epsilon_{\text{max}} = 53\,100\text{ M}^{-1}\text{ cm}^{-1}$ for **KOY-1**) or 400 nm to 480 nm ($\lambda_{\text{max}}^{\text{abs}} = 441$ nm, $\epsilon_{\text{max}} = 50\,800\text{ M}^{-1}\text{ cm}^{-1}$ for



KOY-1-BF₃) and 480 nm to 520 nm ($\lambda_{\text{max}}^{\text{abs}} = 498 \text{ nm}$, $\epsilon_{\text{max}} = 67\,600 \text{ M}^{-1} \text{ cm}^{-1}$ for **KOY-1** and $\lambda_{\text{max}}^{\text{abs}} = 498 \text{ nm}$, $\epsilon_{\text{max}} = 64\,600 \text{ M}^{-1} \text{ cm}^{-1}$ for **KOY-1-BF₃**); the former and later are assigned to the ICT excitation from the electron-donating moiety (carbazole skeleton) to the electron-accepting moiety (pyridyl groups for **KOY-1** and pyridyne-BF₃ units for **KOY-1-BF₃**) and the BODIPY skeleton, respectively. For the corresponding fluorescence spectra, **D1** shows a fluorescence band with a fluorescence maximum ($\lambda_{\text{max}}^{\text{fl}}$) at 436 nm in the range of 420 nm to 550 nm with photoexcitation at 400 nm. For **D1-BF₃**, on the other hand, there is no detectable fluorescence spectrum. **A1** exhibits a $\lambda_{\text{max}}^{\text{fl}}$ at 514 nm originating from the BODIPY skeleton by the photoexcitation at 400 nm and 470 nm. It is worth mentioning here that the photoabsorption spectrum (420–520 nm) of acceptor fluorophore **A1** has spectral overlap with the fluorescence spectrum (420–550 nm) of donor fluorophore **D1** (Fig. S28, SI). The fact suggests that for **KOY-1** the FRET from the D-(π -A)₂ skeleton as the donor fluorophore to the BODIPY skeleton as the acceptor fluorophore occurs by the photoexcitation using the ICT-based $\lambda_{\text{max}}^{\text{abs}}$ of the D-(π -A)₂ skeleton (**D1** moiety), leading to fluorescence emission originating from the BODIPY skeleton. In fact, **KOY-1** exhibits two fluorescence bands with the $\lambda_{\text{max}}^{\text{fl}}$ at 450 nm and the $\lambda_{\text{max}}^{\text{fl}}$ at 516 nm originating from the D-(π -A)₂ skeleton and the BODIPY skeleton, respectively, by the photoexcitation ($\lambda^{\text{ex}} = 400 \text{ nm}$) corresponding to both the ICT-based photoabsorption of D-(π -A)₂ skeleton and the feeble and broad photoabsorption band of the BODIPY skeleton, although **KOY-1** shows an only fluorescence band with the $\lambda_{\text{max}}^{\text{fl}}$ at 515 nm originating from the BODIPY skeleton by the photoexcitation ($\lambda^{\text{ex}} = 470 \text{ nm}$) of the BODIPY skeleton (Fig. S26a, SI). However, this result indicates that the FRET efficiency for **KOY-1** is not quantitative by the fact that the two fluorescence bands originating from both the D-(π -A)₂ skeleton and the BODIPY skeleton were observed. Thus, we estimated the FRET efficiency for **KOY-1** from the equation $E_{\text{FRET}} = 1 - (\tau_{\text{DA}}/\tau_{\text{D}})$ based on time-resolved fluorescence lifetime measurements, where τ_{DA} and τ_{D} are the donor fluorescence lifetimes in the presence and absence of an acceptor, that is, τ_{DA} and τ_{D} are the fluorescence lifetimes of **KOY-1** (0.96 ns) and **D1** (1.70 ns), respectively, in acetonitrile. The FRET efficiency (E_{FRET} value) for **KOY-1** in the absolute acetonitrile solution was evaluated to be 44%. The reason for the low E_{FRET} value of **KOY-1** might be not only intense fluorescence emission originating from the D-(π -A)₂ skeleton (actually, the fluorescent quantum yield Φ_{fl} of **D1** is 76% in absolute acetonitrile) that is too strong for the BODIPY skeleton to well absorb the energy, but also poor overlap integral of the donor fluorescence spectrum with the acceptor photoabsorption spectrum. Meanwhile, **KOY-1-BF₃** exhibits a single fluorescence band with the $\lambda_{\text{max}}^{\text{fl}}$ at 517 nm originating from the BODIPY skeleton by both the photoexcitation ($\lambda^{\text{ex}} = 400 \text{ nm}$) of the D-(π -A)₂ and BODIPY skeletons and the photoexcitation ($\lambda^{\text{ex}} = 470 \text{ nm}$) of only the BODIPY skeleton (Fig. S26c, SI), which is not due to the FRET process but due to the photoexcitation of the BODIPY

skeleton because the **D1-BF₃** skeleton exhibits no fluorescence emission. Nevertheless, it is expected that the addition of water to the **KOY-1-BF₃** solution causes its dissociation into thienylpyridine-carbazole-based D-(π -A)₂ fluorophore **KOY-1** and then the energy transfer from the D-(π -A)₂ skeleton to the BODIPY skeleton through the FRET process, and thus resulting in the enhancement of fluorescence emission originating from the BODIPY skeleton. In addition, it was found that the pseudo-SS value of **KOY-1** between the $\lambda_{\text{max}}^{\text{abs}}$ of the D-(π -A)₂ skeleton and the $\lambda_{\text{max}}^{\text{fl}}$ of the BODIPY skeleton is 7942 cm^{-1} (150 nm), which is significantly higher than that (3945 cm^{-1} ; 64 nm) of **D1** and that (665 cm^{-1} ; 17 nm) of **A1**.

Optical sensing ability for water

In order to investigate the optical sensing ability of **KOY-1-BF₃** for water in a solvent, the photoabsorption and fluorescence spectra of **D1**, **D1-BF₃**, **A1** and **KOY-1** as well as **KOY-1-BF₃** were measured in acetonitrile or THF containing various concentrations of water (Fig. 4). For **KOY-1-BF₃**, the ICT-based photoabsorption band at around 440 nm decreases with the simultaneous increase in a photoabsorption band at around 360 nm, which is assignable to the ICT-based photoabsorption band of **KOY-1** with the increase in the water content in the acetonitrile solution (Fig. 4a and c). On the other hand, the photoabsorption band at around 500 nm originating from the BODIPY skeleton shows unnoticeable changes upon addition of water to the acetonitrile solution.

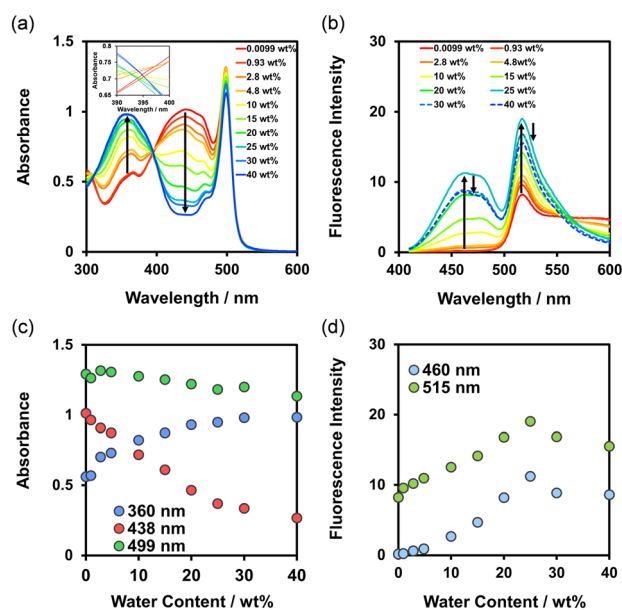


Fig. 4 (a) Photoabsorption and (b) fluorescence spectra ($\lambda^{\text{ex}} = 400 \text{ nm}$) of **KOY-1-BF₃** ($c = 2.0 \times 10^{-5} \text{ M}$) in acetonitrile containing water (0.0099–40 wt%). Inset in (a) is magnification of the spectrum around 395 nm. (c) Absorbance at 360 nm, 438 nm and 499 nm of **KOY-1-BF₃** as a function of the water content (0.0099–40 wt%) in acetonitrile. (d) Fluorescence peak intensity at 460 nm and 515 nm of **KOY-1-BF₃** ($\lambda^{\text{ex}} = 400 \text{ nm}$) as a function of the water content (0.0099–40 wt%) in acetonitrile.



The decrease and increase in the two ICT-based photoabsorption bands level off in the water content region greater than 40 wt%, but it should be noticed that the existence of the isosbestic point was not observed in the water content range from 0.0099 wt% (absolute acetonitrile) to 40 wt% (Fig. 4a inset), although the absorbance at around 400 nm does not appear to change. Thus, the absence of the isosbestic point indicates the presence of three or more chemical species, that is, two or more reactions and equilibria occur upon addition of water to the sensor solution.^{63,64} The corresponding fluorescence spectra of **KOY-1-BF₃** exhibited the appearance and enhancement of a fluorescence emission band at around 460 nm as well as the enhancement of fluorescence emission intensity at around 515 nm originating from the BODIPY skeleton in the water content region below 25 wt%, and then underwent a decrease in the intensity of both the fluorescence emission bands in the water content region over 30 wt% (Fig. 4b and d). Actually, for **KOY-1-BF₃** in the acetonitrile solution containing the water content of 25 wt%, the photoabsorption spectrum (420–520 nm) originating from the BODIPY skeleton has spectral overlap with the fluorescence spectrum (420–550 nm) originating from the D-(π -A)₂ skeleton (Fig. S28, SI). The fact strongly indicated that the addition of water to the **KOY-1-BF₃** solution causes its dissociation into thienylpyridine-carbazole-based D-(π -A)₂ fluorophore **KOY-1** and then the FRET process from the excited-state donor fluorophore D-(π -A)₂ skeleton to the acceptor fluorophore BODIPY skeleton. In fact, it was confirmed that removing water from the **KOY-1-BF₃** acetonitrile solution containing water does not recover to the original **KOY-1-BF₃**. Meanwhile, as with the case of **YNI-2**, the photoabsorption spectra of **D1** showed a slight bathochromic shift upon the addition of water to the THF solution (Fig. S27a and c, SI). The corresponding fluorescence spectra of **D1** underwent a decrease in the intensity with a red-shift (*ca.* 20 nm) of the fluorescence band at around 440 nm in the water content region over 30 wt% (Fig. S27b and d, SI), and it is attributed to the formation of the hydrogen-bonded proton transfer complex (PTC) **D1-H₂O** with water molecules, which shows a feeble fluorescence emission property, as well as the fluorescence solvatochromic property of **D1**.^{19,65} As with the case of **YNI-2-BF₃**, **D1-BF₃** exhibited a decrease in the ICT-based photoabsorption band at around 440 nm with a simultaneous increase in another ICT-based photoabsorption band at round 360 nm, and the appearance and enhancement of a fluorescence emission band at around 490 nm in the water content region below 20 wt%, which is attributed to the change in the ICT characteristics due to the dissociation of **D1-BF₃** into D-(π -A)₂-type pyridine dye **D1** (Fig. 5).¹⁹ In addition, the absence of the isosbestic point upon the addition of water to the solution indicates the presence of the three or more chemical species (Fig. 5a, inset).^{63,64} Furthermore, in the high water content region over 25 wt%, a decrease in the fluorescence intensity was observed due to the formation of **D1-H₂O**. It is worth mentioning here that for **KOY-1** the photoabsorption band

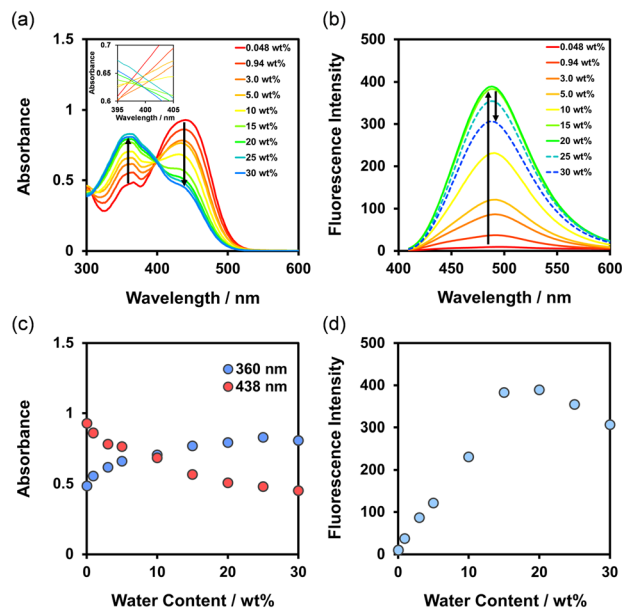


Fig. 5 (a) Photoabsorption and (b) fluorescence spectra ($\lambda^{\text{ex}} = 400$ nm) of **D1-BF₃** ($c = 2.0 \times 10^{-5}$ M) in acetonitrile containing water (0.048–30 wt%) Inset in (a) is magnification of the spectrum around 400 nm. (c) Absorbance at 360 nm and 438 nm of **D1-BF₃** as a function of the water content (0.048–30 wt%) in acetonitrile. (d) Fluorescence peak intensity at 490 nm of **D1-BF₃** ($\lambda^{\text{ex}} = 400$ nm) as a function of the water content (0.048–30 wt%) in acetonitrile.

with $\lambda_{\text{max}}^{\text{abs}}$ at 366 nm showed a slight bathochromic shift, but at photoabsorption band with $\lambda_{\text{max}}^{\text{abs}}$ at 498 nm did not undergo appreciable changes, upon addition of water to the acetonitrile solution (Fig. 6a and c). Meanwhile, the corresponding fluorescence spectra by the photoexcitation at 400 nm underwent a decrease in the intensity of the two fluorescence bands with the $\lambda_{\text{max}}^{\text{fl}}$ at 460 nm and the $\lambda_{\text{max}}^{\text{fl}}$ at 515 nm originating from the D-(π -A)₂ skeleton and the BODIPY skeleton, respectively, with the increase in the water content in the acetonitrile solution (Fig. 6b and d). On the other hand, the photoabsorption and fluorescence spectra of **A1** did not undergo appreciable changes upon the addition of water to the acetonitrile solution (Fig. S27e–h, SI). These results suggest that the resulting **KOY-1**, produced by adding water to the **KOY-1-BF₃** solution, may induce the formation of the hydrogen-bonded PTC **KOY-1-H₂O** with water molecules, which shows a feeble fluorescence emission property. Consequently, these results indicated that the amount of water over a wide range from the low water content to the high water content in solvents can be quantified by both the changes in absorbance at 438 nm originating from the ICT characteristics and fluorescence intensity at 515 nm originating from the BODIPY skeleton.

Furthermore, in order to investigate whether the optical response of **KOY-1-BF₃** is specific to water, we have performed the photoabsorption and fluorescence spectral measurements of **KOY-1-BF₃** in acetonitrile containing ethanol (0–40 wt%) as a protic solvent (Fig. S29, SI). It was found that the changes in the photoabsorption and fluorescence spectra of **KOY-1-BF₃** upon the addition of



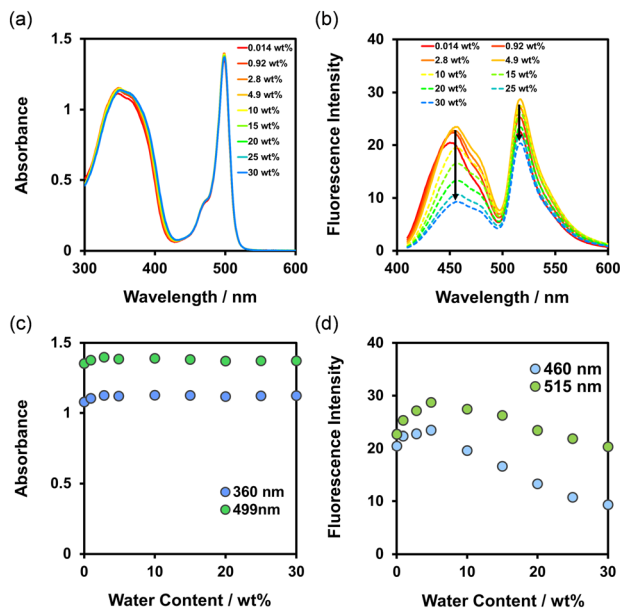


Fig. 6 (a) Photoabsorption and (b) fluorescence spectra ($\lambda^{\text{ex}} = 400$ nm) of **KOY-1** ($c = 2.0 \times 10^{-5}$ M) in acetonitrile containing water (0.014–30 wt%). (c) Absorbance at 360 nm and 499 nm of **KOY-1** as a function of the water content (0.014–30 wt%) in acetonitrile. (d) Fluorescence peak intensity at 460 nm and 515 nm of **KOY-1** ($\lambda^{\text{ex}} = 400$ nm) as a function of the water content (0.014–30 wt%) in acetonitrile.

ethanol are small compared to the case of the addition of water. This result demonstrated that the ICT/FRET-type fluorescent sensor **KOY-1-BF₃** exhibits a somewhat selective optical response to water.

On the basis of the above results, we considered the optical sensing ability of **KOY-1-BF₃** for water in acetonitrile. The E_{FRET} value for **KOY-1-BF₃** in acetonitrile solution containing the water content of 25 wt% corresponding to the maximum fluorescence intensity in the fluorescence enhancement process upon the addition of water is estimated to be 49%, where τ_{DA} and τ_{D} are the fluorescence lifetimes of **KOY-1-BF₃** (0.85 ns) and **D1-BF₃** (1.68 ns), respectively, in acetonitrile containing the water content of 25 wt% or 20 wt%. Indeed, the E_{FRET} value (49%) is similar with that of **KOY-1** in the absolute acetonitrile solution ($E_{\text{FRET}} = 44\%$). Furthermore, the E_{FRET} value (29%) for **KOY-1-BF₃** in acetonitrile solution containing the water content of 40 wt% which corresponds to the minimum fluorescence intensity in the fluorescence attenuation process from the maximum fluorescence intensity upon addition of water, were estimated from the τ_{DA} value (0.77 ns) for **KOY-1-BF₃** and the τ_{D} value (1.08 ns) for **D1-BF₃** in acetonitrile containing the water content of 40 wt% or 30 wt%. It is worth noting here that the E_{FRET} value (29%) for **KOY-1-BF₃** in the acetonitrile solution containing the water content of 40 wt% is lower than that (44%) for **KOY-1** in the absolute acetonitrile solution. Consequently, the fact doubtlessly indicates that the addition of water to the **KOY-1-BF₃** solution causes its dissociation into thienylpyridine-carbazole-based D-(π -A)₂ fluorophore

KOY-1 and then the energy transfer from the excited-state donor fluorophore D-(π -A)₂ skeleton (**D1** structure) to the acceptor fluorophore BODIPY skeleton (**A1** structure) through the FRET process, and thus resulting in a large pseudo-SS and an enhancement of fluorescence emission originating from the BODIPY skeleton. As with case of **YNI-2-BF₃**, in the high water content region, the resulting **KOY-1** may induce the formation of the hydrogen-bonded proton transfer complex (PTC) **KOY-1-H₂O** with water molecules, which shows a feeble fluorescence emission property, leading to a decrease in the fluorescence intensity due to the relatively low FRET efficiency, as well as the fluorescence solvatochromic property of **KOY-1**.

Thus, in order to estimate the sensitivity and accuracy characteristics of **KOY-1-BF₃** as an ICT/FRET-type fluorescent sensor for the detection of water in acetonitrile, the changes in fluorescence intensity at 460 nm and 515 nm are plotted against the water fraction below 25 wt% in acetonitrile (Fig. 7a). The plots demonstrated that the fluorescence peak intensity at 460 nm and 515 nm increased linearly as a function of the water content. Indeed, the correlation coefficient (R^2) values for the two calibration curves are 0.99 and 0.96, respectively, which indicates the good linearity. Therefore, the detection limit (DL) was determined from the plot of the fluorescence intensity at 460 nm and 515 nm versus water fraction in the low water content region below 25 wt% (DL = $3.3\sigma/m_s$, where σ is the standard deviation of

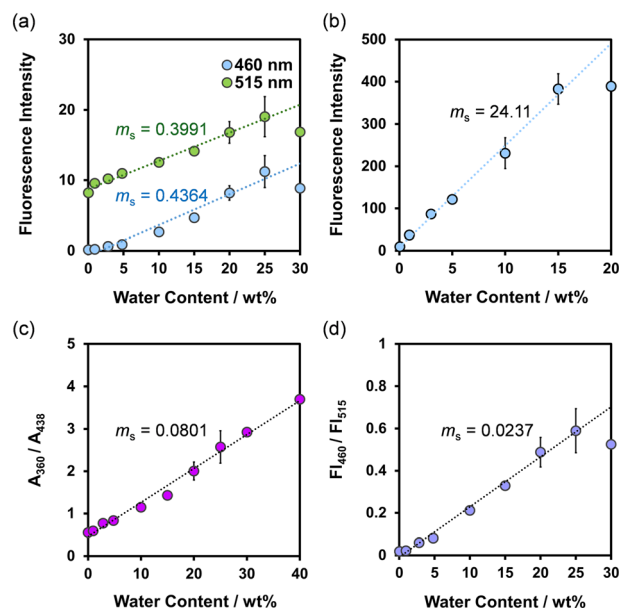


Fig. 7 (a) Fluorescence peak intensity at 460 nm and 515 nm of **KOY-1-BF₃** ($\lambda^{\text{ex}} = 400$ nm) as a function of water content below 25 wt% in acetonitrile. (b) Fluorescence peak intensity at 490 nm of **D1-BF₃** ($\lambda^{\text{ex}} = 400$ nm) as a function of water content below 15 wt% in acetonitrile. (c) Ratio (A_{360}/A_{438}) of absorbance at 360 nm to that at 438 nm of **KOY-1-BF₃** as a function of water content below 40 wt% in acetonitrile. (d) Ratio (FL_{460}/FL_{515}) of fluorescence intensity at 460 nm to 515 nm of **KOY-1-BF₃** as a function of water content below 25 wt% in acetonitrile.



the blank sample and m_s is the slope of the calibration curve in the water content region below 25 wt%). The DL values for the fluorescence intensity at 460 nm and 515 nm are estimated to be 7.56 wt% and 8.27 wt%, respectively, that are inferior to that (0.14 wt%) of **D1-BF₃** (Fig. 7b) and those (0.018–0.25 wt%) of recently reported ICT-type, ESIPT-type, PET-type, FRET-type, and PET/FRET-type fluorescent sensors (Table S1, SI). The inferior DL value of **KOY-1-BF₃** may be attributed to the dynamic motion of the phenylene spacer between donor (**D1** moiety) and acceptor (**A1** moiety) fluorophores, leading to the non-radiative decay of the photoexcited BODIPY fluorophore (**A1** moiety). In fact, the Φ_{fl} value (<1%) of **KOY-1-BF₃** in acetonitrile with 25 wt% water content significantly is lower than that (12%) of **D1-BF₃** in acetonitrile with the 15 wt% water content, although the acceptor fluorophore **A1** shows a moderate Φ_{fl} value (45%) in acetonitrile with and without the water content. Thus, this result suggests that the DL values of the ICT/FRET-type fluorescent sensor can be improved by using a rigid spacer such as an acetylene group to increase the Φ_{fl} value and by using a donor and acceptor fluorophores exhibiting good overlap integral of the donor fluorescence spectrum with the acceptor photoabsorption spectrum to enhance the FRET efficiency. Moreover, the ratio (A_{360}/A_{438}) of absorbance at 360 nm to that at 438 nm and the ratio (F_{460}/F_{515}) of fluorescence intensity at 460 nm to that at 515 nm are plotted against the water fraction below 40 wt% and 25 wt%, respectively, in acetonitrile (Fig. 7c and d). The two plots showed a good linear relationship with the R^2 values of 0.99, indicating ICT/FRET-type fluorescent sensor possessing large pseudo-SS is capable of detecting water in colorimetric and ratiometric fluorescent analysis. The fact also strongly indicates that the fluorescence sensing mechanism of **KOY-1-BF₃** for water is based on the change in the ICT characteristics and occurrence of FRET with the increase in the water content in solvent.

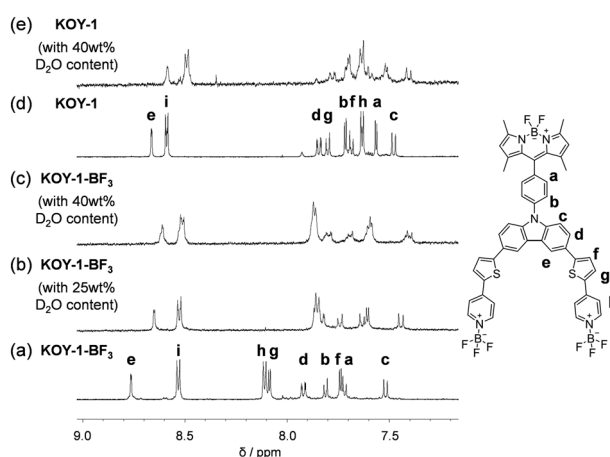


Fig. 8 ^1H NMR spectra of **KOY-1-BF₃** in acetonitrile- d_3 (a) without the addition of D_2O , and with (b) 25 wt% and (c) 40 wt% D_2O content. ^1H NMR spectra of **KOY-1** in acetonitrile- d_3 (d) without the addition of D_2O and (e) with 40 wt% D_2O content.

Optical sensing mechanism for water

In order to confirm the mechanism for the detection of water in solvent based on the ICT/FRET characteristics of **KOY-1-BF₃**, we performed ^1H and ^{11}B NMR spectral measurement of **KOY-1-BF₃** and **KOY-1** with and without the addition of deuterium oxide (D_2O) in acetonitrile- d_3 . For the ^1H NMR spectrum of **KOY-1-BF₃** in acetonitrile- d_3 without the addition of D_2O (Fig. 8a), it was observed that the chemical shifts of the aromatic protons on the two thienylpyridine moieties as well as the carbazole skeleton show a downfield shift compared to those for **KOY-1** in acetonitrile- d_3 without the addition of D_2O (Fig. 8d), as with the cases of **YNI-2-BF₃** and **YNI-2** (Fig. 1). On the other hand, the ^1H NMR spectrum of **KOY-1-BF₃** in acetonitrile- d_3 with the D_2O content of 25 wt% (Fig. 8b), which corresponds to the maximum fluorescence intensity in the fluorescence enhancement process, is similar to that of **KOY-1** in acetonitrile- d_3 without the addition of D_2O (Fig. 8d). Indeed, this result demonstrates the dissociation of **KOY-1-BF₃** into **KOY-1** by water molecules. Moreover, the ^1H NMR spectrum of **KOY-1-BF₃** in acetonitrile- d_3 with the D_2O content of 40 wt% (Fig. 8c), which corresponds to the fluorescence attenuation process from the maximum fluorescence intensity upon addition of water, is broadened, compared to that of **KOY-1-BF₃** in acetonitrile- d_3 with the D_2O content of 25 wt% (Fig. 8b), but is similar to that of **KOY-1** in the acetonitrile- d_3 solution with D_2O content of 40 wt% (Fig. 8e). The ^1H NMR spectrum of **KOY-1-BF₃** in acetonitrile- d_3 with the water content of 40 wt% may indicate the existence of another chemical species in a polar protic solvent environment as well as the formation of **KOY-1**. In addition, the ^{11}B NMR spectrum of **KOY-1-BF₃** showed that the signal (at around -0.6 ppm) of boron trifluoride (BF_3) coordinated to the pyridine ring becomes relatively weaker than the signal (at around 1.3 ppm) of (N_2BF_2) in the BODIPY skeleton with the increase in the D_2O content (Fig. 9). It is worth noting here that with the addition of D_2O , the signal which is

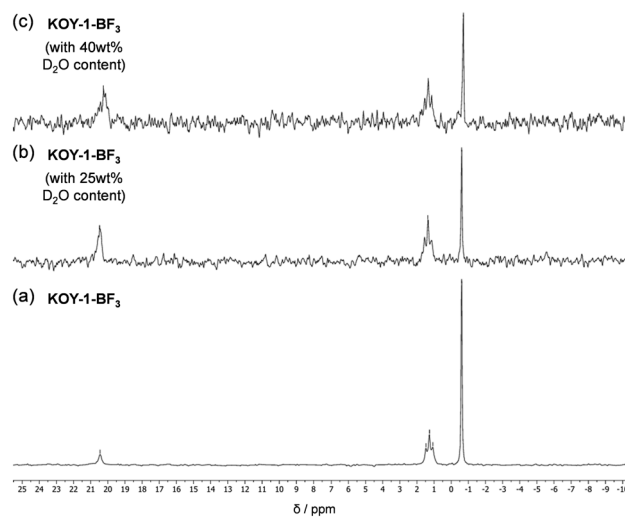


Fig. 9 ^{11}B NMR spectra of **KOY-1-BF₃** in acetonitrile- d_3 (a) without the addition of D_2O , and with (b) 25 wt% and (c) 40 wt% D_2O content.



assignable to boric acid ($B(OD)_3$) that would be produced by the reaction of BF_3 with D_2O appeared at around 20 ppm. This result also strongly indicates the dissociation of $KOY-1-BF_3$ into $KOY-1$ by water molecules.

Thus, the 1H and ^{11}B NMR spectral measurements of $KOY-1-BF_3$ in acetonitrile with and without the addition of water revealed that in the relatively low water content region, $KOY-1-BF_3$ causes its dissociation into the thienylpyridine-carbazole-based $D-(\pi-A)_2$ -BODIPY fluorophore $KOY-1$ and BF_3 (Fig. 10), resulting in the blue-shift of ICT-based photoabsorption and the enhancement of fluorescence emission originating from the BODIPY skeleton through the FRET process between the excited-state donor fluorophore $D-(\pi-A)_2$ skeleton and acceptor fluorophore BODIPY skeleton. Under these experimental conditions, we could not detect the chemical species with the mono pyridine- BF_3 unit, which may be formed by the dissociation of one BF_3 unit from $KOY-1-BF_3$. Thus, the fact suggests that $KOY-1$ is more stable than the chemical species with the mono pyridine- BF_3 unit, leading to rapid and preferential dissociation of $KOY-1-BF_3$ into $KOY-1$, as with the case of $YNI-2-BF_3$.¹⁹ Moreover, in the relatively high water content region, the resulting $KOY-1$ induces the formation of the hydrogen-bonded proton transfer complex (PTC) $KOY-1-H_2O$ between the pyridinic nitrogen atom of $KOY-1$ and the hydroxyl group of water molecules (Fig. 10). Thus, the decrease in fluorescence intensity in the relatively high water content region is attributed to not only the formation of $KOY-1-H_2O$, which shows a feeble fluorescence emission property, but also the fluorescence solvatochromism due to the ICT characteristics of $KOY-1$, leading to a relatively low FRET efficiency. In addition, the absence of isosbestic point in the photoabsorption spectra with the increase in the water content also indicates the presence of the three or more chemical species,^{63,64} that is, $KOY-1$ and $KOY-1-H_2O$, including $KOY-1-BF_3$.

As shown in Fig. 10, the color of $YNI-2-BF_3$ in acetonitrile is orange. Upon the addition of water, the solution changed from orange to nearly colorless due to the dissociation of

$KOY-1-BF_3$ into $KOY-1$. Meanwhile, the fluorescent color for the absolute acetonitrile solution of $KOY-1-BF_3$ seems to be yellow, but the solution containing the water content exhibited intense light blue fluorescence emission originating from the thienylpyridine-carbazole-based $D-(\pi-A)_2$ and BODIPY skeletons due to the formation of $KOY-1$. However, the acetonitrile solution with the high water content shows greenish blue fluorescence emission due to the relatively low FRET efficiency by the hydrogen-bonded PTC ($KOY-1-H_2O$) with water molecules as well as the fluorescence solvatochromic property of $KOY-1$. Consequently, this work demonstrates that $KOY-1-BF_3$ composed of an ICT-type donor fluorophore and an acceptor fluorophore in the FRET process can act as a colorimetric and fluorescent sensor based on the ICT/FRET mechanism for the detection of water over a wide range from the low water content to high water content in solvents.

Conclusions

We have newly designed and developed a ICT/FRET-type colorimetric and fluorescent sensor $KOY-1-BF_3$ possessing a large pseudo-SS for detection of water in solvents; $KOY-1-BF_3$ is composed of a ICT-type donor fluorophore (thienylpyridine-carbazole-based $D-(\pi-A)_2$ skeleton) and an acceptor fluorophore (BODIPY skeleton) in the FRET process. It was found that in the low water content region, $KOY-1-BF_3$ causes its dissociation into thienylpyridine-carbazole-based $D-(\pi-A)_2$ -BODIPY fluorophore $KOY-1$ and BF_3 , leading to the blue-shift of the ICT-based photoabsorption band due to the change in the ICT characteristics and enhancement of fluorescence emission originating from the BODIPY skeleton by occurrence of FRET from the excited-state donor fluorophore $D-(\pi-A)_2$ skeleton to the acceptor fluorophore BODIPY skeleton. Moreover, the decrease in fluorescence intensity in the high water content region is attributed to not only the formation of the hydrogen-bonded proton transfer complex (PTC) $KOY-1-H_2O$ with water molecules, which shows a feeble fluorescence emission property, but also the fluorescence solvatochromism due to the ICT characteristics of $KOY-1$, leading to a relatively low FRET efficiency. Consequently, it was demonstrated that the ICT/FRET-type colorimetric and fluorescent sensor $KOY-1-BF_3$ possesses a large pseudo-SS of 7942 cm^{-1} (150 nm) and moderate FRET efficiency (49%). We anticipate that this work will provide one of the most promising fluorescence enhancement (turn-on) system with a large Stokes shift for the detection of water and lead to the creation of functional materials as well as colorimetric and fluorescent methods to enable visualization and quantification of water.

Author contributions

Y. O. conceived the project. K. I. directed the experimental work. K. O. performed most of the experiments.

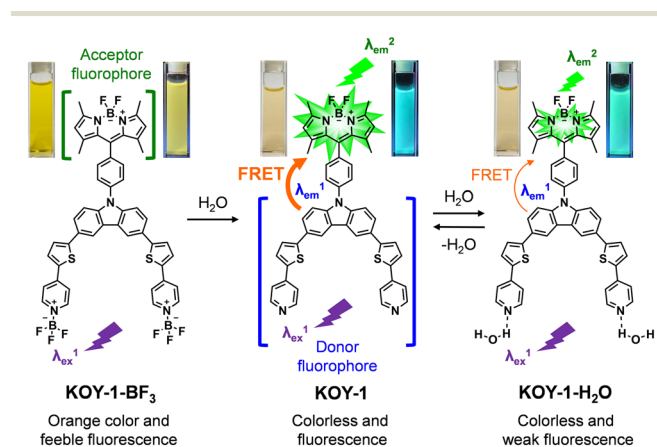


Fig. 10 Proposed mechanisms of ICT/FRET-type colorimetric and fluorescent sensor $KOY-1-BF_3$ for the detection of water in solvent; inset: color (left) and fluorescence color (right) images (under 365 nm irradiation).



Conflicts of interest

The authors declare that there are no conflicts of interest.

Data availability

The data that support the findings of this work are available in the supplementary information (SI).

Supplementary information: details of the experimental methods, additional figures and tables. See DOI: <https://doi.org/10.1039/d6sd00055j>.

Acknowledgements

This work was supported by the Japan Society for the Promotion of Science (JSPS) KAKENHI Grant Number 25K01808 and 25K22857 and by the Toshiaki Ogasawara Memorial Foundation.

References

- 1 R. Wernecke and J. Wernecke, *Industrial Moisture and Humidity Measurement*, Wiley-VCH, Weinheim, 2013.
- 2 L.-O. Nilsson, *Methods of Measuring Moisture in Building Materials and Structures*, Springer, Switzerland, 2018.
- 3 M. Liu, X. Zheng, M. Zhang, S. Yao, P. Zhang, L. Lianga and Y. C. Chen, *Chem. Commun.*, 2026, **62**, 1572–1575.
- 4 M. Chandrakanth, K. Fabitha, P. C. A. Swamy and J. Banothu, *New J. Chem.*, 2026, **50**, 3026–3036.
- 5 J. Issac, R. R. Priyadharsan, K. Chidambaranathan, S. Karthikeyan, D. Moon, S. P. Anthony and V. Madhu, *RSC Adv.*, 2025, **15**, 44205–44212.
- 6 Y. Ida, K. Imato and Y. Ooyama, *New J. Chem.*, 2025, **49**, 19950–19954.
- 7 D. Han, H. Liu, Y. Liu, Y. Zhang, G. Suna and J. Wang, *New J. Chem.*, 2025, **49**, 12523–12531.
- 8 S. Mishra and A. K. Singh, *Coord. Chem. Rev.*, 2021, **445**, 214063.
- 9 H. S. Jung, P. Verwilt, W. Y. Kim and J. S. Kim, *Chem. Soc. Rev.*, 2016, **45**, 1242–1256.
- 10 P. P. Dash, A. K. Ghosh, P. Mohanty, R. Behura, S. Behera, B. R. Jali and S. K. Sahoo, *Talanta*, 2024, **275**, 126089.
- 11 W.-E. Lee, Y.-J. Jin, L.-S. Park and G. Kwak, *Adv. Mater.*, 2012, **24**, 5604–5609.
- 12 J. Lee, M. Pyo, S. Lee, J. Kim, M. Ra, W.-Y. Kim, B. J. Park, C. W. Lee and J.-M. Kim, *Nat. Commun.*, 2014, **5**, 3736.
- 13 A. Morimoto, K. Shimizu, N. Suzuki, S. Yagi, K. Sueyoshi, T. Endo and H. Hisamoto, *Analyst*, 2024, **149**, 1939–1946.
- 14 G. Das, F. A. Ibrahim, Z. A. Khalil, P. Bazin, F. Chandra, R. G. AbdulHalim, T. Prakasam, A. K. Das, S. K. Sharma, S. Varghese, S. Kirmizialtin, R. Jagannathan, N. Saleh, F. Benyettou, M. E. Roz, M. Addicoat, M. A. Olson, D. S. S. Rao, S. K. Prasad and A. Trabolsi, *Small*, 2024, **20**, 2311064.
- 15 J. Wang, Y. Huang, Z. Gao and J. Du, *ACS Appl. Nano Mater.*, 2024, **7**, 7958–7965.
- 16 I. M. Resta and F. Galindo, *Dyes Pigm.*, 2022, **197**, 109908.
- 17 Z. Zhao, Q. Hu, W. Liu, X. Xiong, Z. Wang and H. Wang, *Dyes Pigm.*, 2023, **213**, 111186.
- 18 K. P. Jose, R. R. Priyadharsan, K. Chidambaranathan, S. Karthikeyan, S. P. Anthony and V. Madhu, *Dyes Pigm.*, 2025, **242**, 112926.
- 19 S. Tsumura, T. Enoki and Y. Ooyama, *Chem. Commun.*, 2018, **54**, 10144–10147.
- 20 T. Enoki and Y. Ooyama, *Dalton Trans.*, 2019, **48**, 2086–2092.
- 21 K. Imato, T. Enoki and Y. Ooyama, *RSC Adv.*, 2019, **9**, 31466–31473.
- 22 Y. Dai, H. Gao and H. Huang, *Anal. Methods*, 2025, **17**, 9823–9832.
- 23 A. Ghosh, A. Adhikary and S. Guria, *Chem. – Asian J.*, 2025, **20**, e00778.
- 24 Y. Hong, C. Cui, S. Li, Z. Yan, Q. Zhou, K. Li and Z. Wang, *Anal. Methods*, 2025, **17**, 7033–7045.
- 25 D. Han, H. Liu, Y. Liu, Y. Zhang, G. Suna and J. Wang, *New J. Chem.*, 2025, **49**, 12523–12531.
- 26 J. S. Kim, M. G. Choi, Y. Huh, M. H. Kim, S. H. Kim, S. Y. Wang and S.-K. Chang, *Bull. Korean Chem. Soc.*, 2006, **27**, 2058–2060.
- 27 A. C. Kumar and A. K. Mishra, *Talanta*, 2007, **71**, 2003–2006.
- 28 Y. Ooyama, *Sustainable and Functional Redox Chemistry*, ed. S. Inagi, The Royal Society of Chemistry, Cambridge, UK, ch. 13, 2022, pp. 300–330.
- 29 Y. Ooyama, M. Sumomogi, T. Nagano, K. Kushimoto, K. Komaguchi, I. Imae and Y. Harima, *Org. Biomol. Chem.*, 2011, **9**, 1314–1316.
- 30 Y. Ooyama, A. Matsugasako, K. Oka, T. Nagano, M. Sumomogi, K. Komaguchi, I. Imae and Y. Harima, *Chem. Commun.*, 2011, **47**, 4448–4450.
- 31 Y. Ooyama, A. Matsugasako, Y. Hagiwara, J. Ohshita and Y. Harima, *RSC Adv.*, 2012, **2**, 7666–7668.
- 32 Y. Ooyama, K. Furue, K. Uenaka and J. Ohshita, *RSC Adv.*, 2014, **4**, 25330–25333.
- 33 Y. Ooyama, M. Hato, T. Enoki, S. Aoyama, K. Furue, N. Tsunoji and J. Ohshita, *New J. Chem.*, 2016, **40**, 7278–7281.
- 34 Y. Ooyama, R. Sagisaka, T. Enoki, N. Tsunoji and J. Ohshita, *New J. Chem.*, 2018, **42**, 13339–13350.
- 35 D. Jinbo, K. Imato and Y. Ooyama, *RSC Adv.*, 2019, **9**, 15335–15340.
- 36 D. Jinbo, K. Ohira, K. Imato and Y. Ooyama, *Mater. Adv.*, 2020, **1**, 354–362.
- 37 Y. Mise, K. Imato, T. Ogi, N. Tsunoji and Y. Ooyama, *New J. Chem.*, 2021, **45**, 4164–4173.
- 38 T. Fumoto, S. Miho, Y. Mise, K. Imato and Y. Ooyama, *RSC Adv.*, 2021, **11**, 17046–17050.
- 39 S. Miho, T. Fumoto, Y. Mise, K. Imato, S. Akiyama, M. Ishida and Y. Ooyama, *Mater. Adv.*, 2021, **2**, 7662–7670.
- 40 E. Nishimoto, Y. Mise, T. Fumoto, S. Miho, N. Tsunoji, K. Imato and Y. Ooyama, *New J. Chem.*, 2022, **46**, 12474–12481.
- 41 S. Miho, K. Imato and Y. Ooyama, *RSC Adv.*, 2022, **12**, 25687–25696.
- 42 T. Fumoto, K. Imato and Y. Ooyama, *New J. Chem.*, 2022, **46**, 21037–21046.
- 43 K. Tao, K. Imato and Y. Ooyama, *Sens. Diagn.*, 2024, **3**, 631–639.



- 44 C. C. Ghosh and P. P. Parui, *New J. Chem.*, 2025, **49**, 10420–10428.
- 45 Di Yang, X.-T. Wu, X.-J. Cao and B.-X. Zhao, *Dyes Pigm.*, 2019, **170**, 107558.
- 46 D. Han, H. Liu, Y. Liu, Y. Zhang, G. Suna and J. Wang, *New J. Chem.*, 2025, **49**, 12523–12531.
- 47 F. Khan, A. Ekbote, S. M. Mobin and R. Misra, *J. Org. Chem.*, 2021, **86**, 1560–1574.
- 48 X. Y. Shen, Y. J. Wang, H. Zhang, A. Qin, J. Z. Sun and B. Z. Tang, *Chem. Commun.*, 2014, **50**, 8747–8750.
- 49 L. Ding, Z. Zhang, X. Li and J. Su, *Chem. Commun.*, 2013, **49**, 7319–7321.
- 50 Y. Mise, K. Imato, T. Ogi, N. Tsunoji and Y. Ooyama, *New J. Chem.*, 2021, **45**, 4164–4173.
- 51 Y. Zhang, D. Li, Y. Li and J. Yu, *Chem. Sci.*, 2014, **5**, 2710–2716.
- 52 N. Zhao, Z. Yang, J. W. Y. Lam, H. H. Y. Sung, N. Xie, S. Chen, H. Su, M. Gao, I. D. Williams, K. S. Wong and B. Z. Tang, *Chem. Commun.*, 2012, **48**, 8637–8639.
- 53 K. M. Meghna, M. M. A. Kumar, S. Sarkar and V. M. Biju, *Anal. Methods*, 2026, **18**, 372–388.
- 54 L. He, B. Dong, Y. Liu and W. Lin, *Chem. Soc. Rev.*, 2016, **45**, 6449–6461.
- 55 F. Peng, X. Ai, J. Sun, L. Yang and B. Gao, *Chem. Commun.*, 2024, **60**, 2994–3007.
- 56 Y. Xu, B. Hu, Y. Cui, L. Li, F. Nian, Z. Zhang and W. Wang, *Chem. Commun.*, 2024, **60**, 83–86.
- 57 Z. Tang, H. Huang, Y. Yao, S. Gao, B. Lin, Q. Zong, W. Hu, J. Xu, Y. Wand and L. Guo, *Chem. Commun.*, 2025, **61**, 560–563.
- 58 K. Xu, L. He, X. Yang, Y. Yand and W. Lin, *Analyst*, 2018, **143**, 3555–3559.
- 59 L.-K. Li, Y.-M. Hou, X.-C. Liu, M.-J. Tian, Q.-J. Ma, N.-N. Zhu and S.-Z. Liu, *New J. Chem.*, 2022, **46**, 6596–6602.
- 60 W. Zhang, F. Huo, F. Cheng and C. Yin, *J. Am. Chem. Soc.*, 2020, **142**, 6324–6331.
- 61 F. Xu, J.-H. Kim, H. U. Kim, J.-H. Jang, K. S. Yook, J. Y. Lee and D. H. Hwang, *Macromolecules*, 2014, **47**, 7397–7406.
- 62 Y. Ooyama, S. Inoue, T. Nagano, K. Kushimoto, J. Ohshita, I. Imae, K. Komaguchi and Y. Harima, *Angew. Chem., Int. Ed.*, 2011, **50**, 7429–7433.
- 63 M. D. Cohen and E. Fischer, *J. Chem. Soc.*, 1962, 3044–3052.
- 64 J. Brynstad and G. P. Smith, *J. Phys. Chem.*, 1968, **72**, 296–300.
- 65 C. Reichardt, *Solvents and Solvent Effects in Organic Chemistry*, VCH, Weinheim, 2003.

